Graphene Fibers

International Edition: DOI: 10.1002/anie.201507246
German Edition: DOI: 10.1002/ange.201507246

Macroscopic Graphene Fibers Directly Assembled from CVD-Grown Fiber-Shaped Hollow Graphene Tubes

*Tao Chen and Liming Dai**

Abstract: *Using a copper wire as the substrate for the CVD growth of a hollow multilayer graphene tube, we prepared a macroscopic porous graphene fiber by removing the copper in an aqueous mixture solution of iron chloride ($FeCl_3$, 1 M) and hydrochloric acid (HCl, 3 M) and continuously drawing the newly released graphene tube out of the liquid. The length of the macroscopic graphene fiber thus produced is determined mainly by the length of the copper wire used. The resultant macroscopic graphene fiber with the integrated graphene structure exhibited a high electrical conductivity (127.3 $S\,cm^{-1}$) and good flexibility over thousands bending cycles, showing great promise as flexible electrodes for wearable optoelectronics and energy devices—exemplified by its use as a flexible conductive wire for lighting a LED and a cathode in a fiber-shaped dye-sensitized solar cell (DSSC) with one of the highest energy conversion efficiencies (3.25 %) among fiber-shaped DSSCs.*

High-performance fibers formed from highly aligned one-dimensional polymer chains (e.g., Kevlar fiber) and/or two-dimensional graphitic sheets (e.g., carbon fiber) have been successfully used as high-strength and light-weight structural materials for transportation, civil engineering, and defense.[1] Recently, macroscopic fibers derived from carbon nanomaterials, such as carbon nanotubes (CNTs) and graphene sheets, have attracted considerable attention owing to their unique mechanical, electrical, and thermal properties.[2–17] Consequently, high-performance CNT fibers have been produced by wet-spinning,[2–6] direct chemical vapor deposition synthesis,[7,8] dry-spinning of highly-aligned CNT arrays in the fashion like spinning of cotton or wool.[9–11] Macroscopic graphene fibers reported to date were mostly assembled from graphene oxide sheets, which were generated by liquid-phase exfoliation of graphite in the presence of ultra-strong acid and oxidizer.[12–17] However, the acid oxidation often causes severe structural damage, which greatly decreases the mechanical and electrical properties of the resulting macroscopic "graphene" fiber. A few of graphene fibers have recently been assembled from planar graphene sheets generated by chemical vapor deposition (CVD),[18,19] but the length of the resulting graphene fibers was limited to several centimeters by the small size of the graphene sheets and the high surface tension of the solvent used during the fiber drawing process, and hence their applications were also greatly limited. Until now, it still remains a great challenge to directly assemble graphene sheets into long fibers without significant structural damage of the constituent graphene sheets.

By using copper (Cu) wires as the growth substrate for CVD growing hollow graphene sheets, we now develop a facile method to directly assemble the resultant hollow graphene tubes into macroscopic graphene fibers of tens of centimeters long without much structural damage. The length of the macroscopic graphene fiber thus produced is determined mainly by the length of the copper wire used, which is unlimited in principle. Figure S1 in the Supporting Information schematically shows the route to a macroscopic graphene fiber drawn from the CVD-grown hollow graphene tubes. To start with, multi-layer graphene hollow tubes were grown on Cu wires with a diameter of 0.64 mm and different lengths (Figure S2 a) by CVD of methane under argon (Ar, 200 sccm) and hydrogen (H_2, 40 sccm) at 1000 °C for 10 min (see Experimental Section). Thereafter, the Cu substrate was removed by etching in an aqueous mixture solution of iron chloride ($FeCl_3$, 1 M) and hydrochloric acid (HCl, 3 M), leading to a hollow graphene tube floating at the liquid/air interface (Figure S2 b–d). The $FeCl_3$ and $CuCl_2$ residue, if any, was removed by repeatedly transferring the hollow graphene into a deionized water for at least five times (see Figure S6 and Table S1). Finally, the graphene fiber with a porous structure formed (see Figure 2 a–d) as the hollow graphene tube was drawn out from water. Graphene fibers with a twisted structure can also be prepared by using a rotating probe for the drawing process.

Figure 1 shows typical scanning electron microscope (SEM) images of a Cu wire before and after the growth of graphene, at different magnifications. A uniform graphene layer on the Cu wire surface is evident in Figure 1 d. The transmission electron microscope (TEM) image given in Figure S3 reveals about ten graphitic layers for the CVD-grown graphene tube with a hexagonal electron diffraction pattern (inset of Figure S3). Compared to conventional multiwalled carbon nanotubes, the large diameter graphene tubes with a few graphene layers have an extremely small wall thickness to tube diameter ratio, and hence a much higher surface area.

As can be seen in Figure 2 a–d, the diameter of the resultant graphene fiber decreased as the graphene tube was

[*] Dr. T. Chen, Prof. Dr. L. Dai
Center of Advanced Science and Engineering for Carbon
Department of Macromolecular Science and Engineering
Case Western Reserve University
10900 Euclid Avenue, Cleveland, OH, 44106 (USA)
E-mail: liming.dai@case.edu
Dr. T. Chen
Current address: Department of Chemistry, Tongji University
Shanghai, 200092 (China)

Supporting information for this article is available on the WWW under http://dx.doi.org/10.1002/anie.201507246.

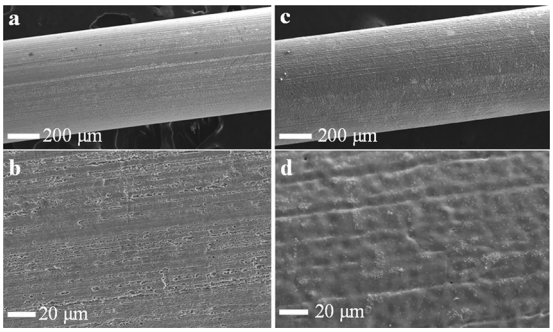

Figure 1. Surface morphologies of the Cu wire before and after the growth of graphene layer. a,b) SEM images of the bare copper wire after treatment with HCl at a low and high magnification. c,d) SEM images of the copper wire after CVD growth of graphene at a low and high magnification.

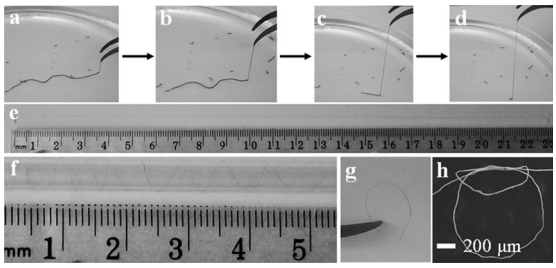

Figure 2. Digital photographs and SEM images of the graphene fibers. a–d) Digital photographs of a graphene fiber formed by drawing a hollow graphene tube out of water. e) A digital photograph of a graphene fiber over 20 cm long. f) A digital photograph of a graphene fiber wrapped on a glass rod. g) A digital photograph of a planar circle with a large radius curvature formed by bending a graphene fiber. h) A SEM image of a knot derived from a graphene fiber.

drawn out from water. Graphene fibers with a length over twenty centimeters (Figure 2e) can be easily produced. The length of the graphene fiber thus produced is, in principle, only limited by the length of the Cu wire used as the template. The Cu wire can be bent back and forth (Figure S2a) or rolled up into the tube furnace for the CVD growth to allow for a large-scale production of the graphene fibers. Thus, graphene fibers with various lengths can be easily fabricated (Figure 2e and Figure S4), which are flexible and can be easily wrapped on a glass rod (Figure 2f), bent from a straight line into a circle (Figure 2g) or made into knot (Figure 2h). Like other carbon fibers,[7–12] our graphene fibers can also be bent and twisted together (Figure S5) to show good potentials for a large variety of applications, ranging from wearable to electrochemical devices.

Unlike those graphene fibers obtained from graphene oxide, our graphene fiber was constructed from a single piece of continuous and integrated graphene sheet, as shown in Figure 3a–c, with good mechanical and electrical properties. Similar to the graphene fiber spun from graphene oxide,[12–17] our graphene fiber also had a rough surface (Figure 3a–c) and porous structure (Figure 3d), arising from the large shrinkage occurred (from 640 μm to 12 μm) during the solution drawing and solvent evaporating processes. These structure features

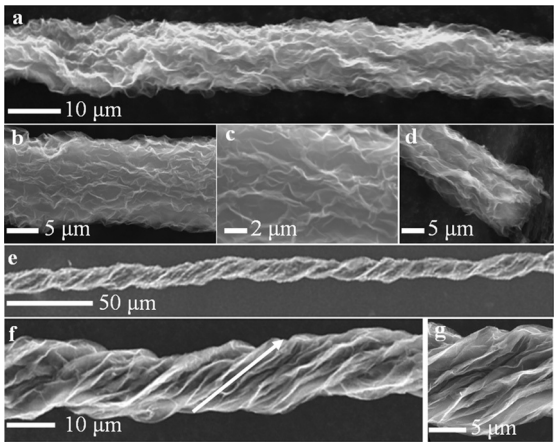

Figure 3. Morphologies of graphene fibers prepared by drawing hollow graphene tubes out of water with and without rotating. a–c) Typical SEM images of a graphene fiber under different magnifications. d) SEM image of the cross-section of the graphene fiber shown in (a). e–g) SEM images of a graphene fiber with the twisted structure produced by using a rotating probe.

made our graphene fibers attractive as fiber electrodes in fiber-shaped energy conversion and storage devices. A twisted graphene fiber with an enhanced mechanical strength can also be formed by adhering the hollow graphene tube onto a rotating probe during the drawing process. Figure 3e–g show SEM images of the graphene fiber with twisted structures, in which the constituent graphene sheet aligned well along the probe rotating direction.

Figure 4a shows Raman spectra for the as-grown graphene on the Cu wire and the corresponding graphene fiber. As expected, both exhibited a strong G-band peak at about 1580 cm^{-1}, relatively weak D-band peak at around 1356 cm^{-1} and 2D peak at about 2720 cm^{-1}. The I_D/I_G ratio (the peak intensity ratio of the D peak versus G peak) of the graphene

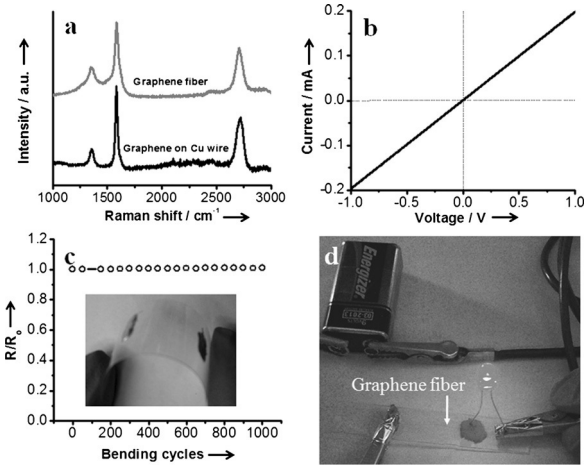

Figure 4. Properties of the graphene fiber. a) Raman spectra of the as-grown graphene on the Cu wire and the resultant graphene fiber. b) I–V curve of a graphene fiber. c) The dependence of electrical resistance of graphene fiber on the bending. d) Digital photograph of a graphene fiber used as one segment conductive wire for lighting a light emitting diode.

fiber was about 0.38, which is much higher than that of the as-grown graphene on the Cu wire (0.21). The above observed difference in the I_D/I_G ratio indicates that some defects have been introduced by the solution drawing process, presumably during the removal of the Cu substrate in the mixture solution of 1 M $FeCl_3$ and 3 M HCl. Both the as-grown graphene on the Cu wire and the resultant graphene fiber showed a similar I_{2D}/I_G ratio of about 0.62, indicating the multilayered nature characteristic of the CVD-grown graphene on a Cu catalyst,[20–22] which is also consistent with our TEM observation (see Figure S3).

The graphene fiber was further evaluated by I–V measurements. Figure 4b shows an Ohmic behavior with an electrical conductivity of 127.3 $S\,cm^{-1}$, calculated according to the equation of $\sigma = L/(RS)$, where R, S, and L represent electrical resistance, the cross-section area, and the length of the graphene fiber, respectively. This value of the conductivity is higher than that of the graphene fiber prepared using multiple pieces of CVD-grown graphene sheets.[18] The high electrical conductivity of our graphene fiber can be attributed to the integrated structure of graphene tube since the residual Cu or Fe, if any, has been largely removed during etching process, as verified by the EDX (energy dispersive X-ray spectroscopy) element analysis (Figure S6 and Table S1). Furthermore, over 1000 bending cycles, up to a bending angle of 60° caused only about 2% change in the electrical resistance of the graphene fiber (Figure 4c), indicating a good mechanical flexibility and electrical stability. To demonstrate the potential application of the graphene fiber, Figure 4d shows that the graphene fiber can be used as a conductive wire for lighting a commercial light emitting diode (3V LED from Microtivity). Owing to its excellent electrical properties, good porosity, and flexibility, the graphene fiber holds great promise as the counter electrode in dye-sensitized solar cells (DSSCs), as discussed below.

Graphene materials have been recently used as metal-free counter electrodes to replace the conventional noble-metal (platinum) electrode in DSSCs.[23–25] Fiber-shaped DSSCs have attracted considerable attentions because of their flexibility and wearability.[26–29] Therefore, we tested our graphene fiber as the counter electrode in fiber-shaped DSSCs. In a typical experiment, a titanium (Ti) wire anodized with a titania nanotube array (Figure S7) was used as the working electrode after being adsorbed with dyes, and the mixture solution of 0.1 M LiI, 0.05 M I_2, 0.6 M dimethyl-3-*n*-propylimidazolium iodide, and 0.5 M 4-tert-butyl-pyridine in dehydrated acetonitrile was used as the redox electrolyte. As schematically shown in Figure 5a, the fiber-shaped DSSC was constructed by assembling the anode Ti wire working electrode together with the graphene fiber counter electrode in parallel, sandwiched with the liquid electrolyte via the capillary force. The ends of the two fiber electrodes were fixed with silver paste for easy and reliable characterization (Figure 5b). Figure 5c schematically shows the working principle for the fiber-shaped DSSC. Briefly, electrons were generated upon light illumination of dye molecules chemisorbed on the titania nanotube electrode. Electrons thus generated were injected into the conduction band of the titania nanotubes, transported to the core titanium wire, and

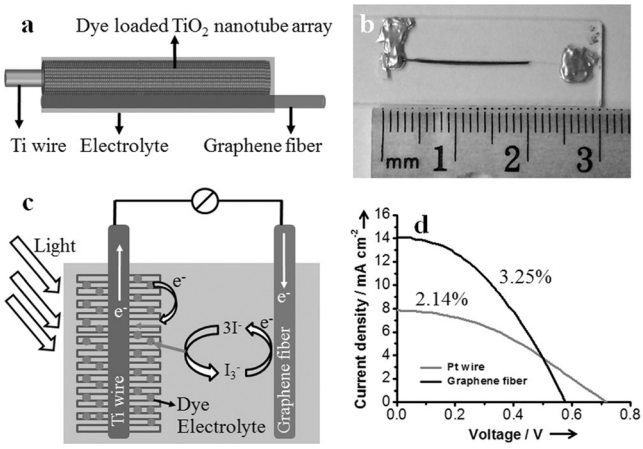

Figure 5. a) Schematic illustration of a fiber-shaped dye-sensitized solar cell using the graphene fiber as the counter electrode. b) A digital photograph of an assembled fiber-shaped dye-sensitized solar cell. c) A schematic illustration of the working principle for the graphene fiber-based dye-sensitized solar cell. d) Current density versus voltage curves of the fiber-shaped dye-sensitized solar cell based on the graphene fiber or platinum wire counter electrodes.

reached the graphene fiber counter electrode through the external circuit. The excited dye molecules were reduced back to the ground state by oxidation of I^- into I_3^- ions, while I_3^- is reduced to I^- by accepting electrons from the graphene fiber to close the electrical circuit. Figure 5d shows the current density versus voltage curve for the fiber-shaped DSSC under the AM 1.5 simulation light, from which a power conversion efficiency of 3.25% was obtained with a short-circuit current density (J_{sc}) of 14.10 $mA\,cm^{-2}$, open-circuit voltage (V_{oc}) of 0.58 V, and fill factor (FF) of 0.40. The observed device performance is comparable to that of the fiber-shaped solar cell based on a CNT-fiber counter electrode reported previously.[29] For comparison, a platinum wire with a diameter of 25 μm was tested as the counter electrode under the same condition, leading to an efficiency of 2.14% (Figure 5d). The higher efficiency for the graphene fiber-based solar cell can be attributable to the higher surface area of graphene than that of the smooth platinum wire, in conjunction with its better electrical and electrochemical properties.

In conclusion, a novel simple approach has been developed to fabricate long and macroscopic graphene fibers with excellent electrical conductivity (over 120.0 $S\,cm^{-1}$) and flexibility by CVD-growing graphene on a Cu wire, followed by removing the Cu template and directly drawing the hollow graphene tube into the graphene fiber. The resultant graphene fiber was demonstrated to show excellent mechanical flexibility and electrical conductivity with the electrical resistance almost unchanged over one thousand bending cycles. Furthermore, fiber-shaped dye-sensitized solar cells based on the newly developed graphene fiber counter electrode were constructed to show an energy conversion efficiency of 3.25%, outperformed its platinum counterparts. The graphene fiber developed in this study holds great promise to be used as fiber electrodes in various electronics beyond DSSCs, such as supercapacitors, sensors, and wearable electronics.

Experimental Section

Copper wire with diameter of 0.64 mm (purchased from Fisher Scientific) was used as the substrate to grow the hollow graphene tube, which was treated prior to the graphene growth by immersing in 3 M HCl aqueous solution for 12 h to remove the oxide layer, followed by washing with deionized water and ethanol three times, respectively, and blow-drying using air gas. Copper wires with different lengths were put into a tube furnace with a diameter of 2 inch, followed by introducing argon (Ar, 200 sccm) and hydrogen (H_2, 40 sccm). The furnace was heated to 1000 °C at a rate of 25 °C min^{-1}, and maintaining at 1000 °C for 10 min. Then, methane was introduced with a flow rate of 10 sccm for the graphene growth around the copper wires at 1000 °C for 10 min. Finally, the zone of the tube for the graphene growth was rapidly moved out of the heating zone (room temperature).

The copper wire after CVD-growth was immersed into an aqueous solution containing 1 M $FeCl_3$ and 3 M HCl overnight to produce a continuous hollow graphene tube floating at the solution/air interface. Then, the hollow graphene tube was carefully contacted onto the tip of tweezers, and transferred into deionized water to remove residue of $FeCl_3$ and $CuCl_2$, if any. This process was repeated five times. Finally, the continuous graphene fiber was directly drawn out from water using tweezers, and the porous structure was formed. The aligned twisted graphene fiber was directly spun out from water by using a rotating probe with speed of 500 rpm.

The aligned TiO_2 nanotube array was grown on the outer surface of Ti wire with a diameter of 127 μm by a two-electrode electrochemical anodization method in the electrolyte of ethylene glycol solution containing 0.25 wt % NH_4F and 2 vol % H_2O at a voltage of 60 V for 4 h, in which Ti wire and platinum plate were used as working electrode and counter electrode, respectively. The anodized Ti wire was washed with deionized water, then annealed at 500 °C in air for 1 h to obtain anatase TiO_2, which was immersed into a solution of 0.3 mM N719 in acetonitrile overnight. The fiber-shaped dye-sensitized solar cell was assembled by putting a dye-sensitized anodized Ti wire and a graphene fiber contacted with each other, followed by dropping on them a liquid electrolyte solution with 0.1 M LiI, 0.05 M I_2, 0.6 M dimethyl-3-*n*-propylimidazolium iodide, and 0.5 M 4-tertbutylpyridine in dehydrated acetonitrile. The liquid electrolyte infiltrated into TiO_2 nanotubes and made the two fibers to contact with each other well because of the capillarity force.

The structure of graphene fiber was characterized by SEM (JEOL JSM-6510LV/LGS operated at 20 kV and Hitachi S4800 at 10 kV). Transmission electron microscopy (TEM) was carried out on a JEOL2100 high-resolution transmission electron microscope at an operation voltage of 200 kV. Raman spectra were collected with the Raman spectroscopy (Renishaw), using 514 nm laser. The solar cell was measured by recording I–V curves with a Keithley 2400 Source Meter under illumination (100 mW cm^{-2}) of simulated AM 1.5 solar light (Oriel-Sol3A 94023A). The effective area of a fiber-solar cell for calculation of the power conversion efficiency was obtained by multiplying the length and diameter of the Ti wire.

Acknowledgements

This work was supported by NSF (DMR-1106160) and DAGSI.

Keywords: conducting materials · dye-sensitized solar cells · flexible electronics · graphene · graphene fibers

How to cite: *Angew. Chem. Int. Ed.* **2015**, *54*, 14947–14950
Angew. Chem. **2015**, *127*, 15160–15163

[1] J. W. S. Hearle, *High-Performance Fibers*, Woodhead, Cambridge, **2000**.
[2] A. B. Dalton, S. Collins, E. Muñoz, J. M. Razal, V. H. Ebron, J. P. Ferraris, J. N. Coleman, B. G. Kim, R. H. Baughman, *Nature* **2003**, *423*, 703.
[3] L. M. Ericson, H. Fan, H. Peng, V. A. Davis, W. Zhou, J. Sulpizio, Y. Wang, R. Booker, J. Vavro, C. Guthy, A. N. G. Parra-Vasquez, M. J. Kim, S. Ramesh, R. K. Saini, C. Kittrell, G. Lavin, H. Schmidt, W. W. Adams, W. E. Billups, M. Pasquali, W. F. Hwang, R. H. Hauge, E. Fischer, R. E. Smalley, *Science* **2004**, *305*, 1447.
[4] B. Vigolo, A. Pénicaud, C. Coulon, C. Sauder, R. Pailler, C. Journet, P. Bernier, P. Poulin, *Science* **2000**, *290*, 1331.
[5] V. A. Davis, A. N. G. Parra-Vasquez, M. J. Green, P. K. Rai, N. Behabtu, V. Prieto, R. D. Booker, J. Schmidt, E. Kesselman, W. Zhou, H. Fan, W. W. Adams, R. H. Hauge, J. E. Fischer, Y. Cohen, Y. Talmon, R. E. Smalley, M. Pasquali, *Nat. Nanotechnol.* **2009**, *4*, 830.
[6] N. Behabtu, C. C. Young, D. E. Tsentalovich, O. Kleinerman, X. Wang, A. W. K. Ma, E. A. Bengio, R. F. ter Waarbeek, J. J. de Jong, R. E. Hoogerwerf, S. B. Fairchild, J. B. Ferguson, B. Maruyama, J. Kono, Y. Talmon, Y. Cohen, M. J. Otto, M. Pasquali, *Science* **2013**, *339*, 182.
[7] Y. Li, I. A. Kinloch, A. H. Windle, *Science* **2004**, *304*, 276.
[8] K. Koziol, J. Vilatela, A. Moisala, M. Motta, P. Cunniff, M. Sennett, A. Windle, *Science* **2007**, *318*, 1892.
[9] K. Jiang, Q. Li, S. Fan, *Nature* **2002**, *419*, 801.
[10] M. Zhang, K. R. Atkinson, R. H. Baughman, *Science* **2004**, *306*, 1358.
[11] M. D. Lima, S. Fang, X. Lepró, C. Lewis, R. Ovalle-Robles, J. Carretero-González, E. Castillo-Martínez, M. E. Kozlov, J. Oh, N. Rawat, C. S. Haines, M. H. Haque, V. Aare, S. Stoughton, A. A. Zakhidov, R. H. Baughman, *Science* **2011**, *331*, 51.
[12] Z. Xu, C. Gao, *Nat. Commun.* **2011**, *2*, 571.
[13] Z. Dong, C. Jiang, H. Cheng, Y. Zhao, G. Shi, L. Jiang, L. Qu, *Adv. Mater.* **2012**, *24*, 1856.
[14] H. Cong, X. Ren, P. Wang, S. Yu, *Sci. Rep.* **2012**, *2*, 613.
[15] Y. Zhao, C. Jiang, C. Hu, Z. Dong, J. Xue, Y. Meng, N. Zheng, P. Chen, L. Qu, *ACS Nano* **2013**, *7*, 2406.
[16] Z. Xu, H. Sun, X. Zhao, C. Gao, *Adv. Mater.* **2013**, *25*, 188.
[17] L. Chen, Y. He, S. Chai, H. Qiang, F. Chen, Q. Fu, *Nanoscale* **2013**, *5*, 5809.
[18] X. M. Li, T. S. Zhao, K. L. Wang, Y. Yang, J. Q. Wei, F. Y. Kang, D. H. Wu, H. W. Zhu, *Langmuir* **2011**, *27*, 12164.
[19] X. Li, T. Zhao, Q. Chen, P. Li, K. Wang, M. Zhong, J. Wei, D. Wu, B. Wei, H. Zhu, *Phys. Chem. Chem. Phys.* **2013**, *15*, 17752.
[20] J. Zhang, P. Hu, X. Wang, Z. Wang, D. Liu, B. Yang, W. Cao, *J. Mater. Chem.* **2012**, *22*, 18283.
[21] D. Graf, F. Molitor, K. Ensslin, C. Stampfer, A. Jungen, C. Hierold, L. Wirtz, *Nano Lett.* **2007**, *7*, 238.
[22] A. C. Ferrari, D. M. Basko, *Nat. Nanotechnol.* **2013**, *8*, 235.
[23] X. Wang, L. Zhi, K. Müllen, *Nano Lett.* **2008**, *8*, 323.
[24] Y. Xue, J. Liu, H. Chen, R. Wang, D. Li, J. Qu, L. Dai, *Angew. Chem. Int. Ed.* **2012**, *51*, 12124; *Angew. Chem.* **2012**, *124*, 12290.
[25] H. Wang, K. Sun, F. Tao, D. J. Stacchiola, Y. H. Hu, *Angew. Chem. Int. Ed.* **2013**, *52*, 9210; *Angew. Chem.* **2013**, *125*, 9380.
[26] T. Chen, L. Qiu, Z. Yang, H. Peng, *Chem. Soc. Rev.* **2013**, *42*, 5031.
[27] X. Fan, Z. Chu, F. Wang, C. Zhang, L. Chen, Y. Tang, D. Zou, *Adv. Mater.* **2008**, *20*, 592.
[28] B. Weintraub, Y. Wei, Z. L. Wang, *Angew. Chem. Int. Ed.* **2009**, *48*, 8981; *Angew. Chem.* **2009**, *121*, 9143.
[29] T. Chen, L. Qiu, H. G. Kia, Z. Yang, H. Peng, *Adv. Mater.* **2012**, *24*, 4623.

Received: August 4, 2015
Published online: October 16, 2015

